Chapter 4

Diffusion of Magnetic Nanoparticles Within a Biological Tissue During Magnetic Fluid Hyperthermia

Mansour Lahonian

Additional information is available at the end of the chapter

http://dx.doi.org/10.5772/52305

1. Introduction

Hyperthermia is one of many techniques used in oncology. It uses the physical methods to heat certain organ or tissue delivering an adequate temperature in an appropriate period of time (thermal dose), to the entire tumor volume for achieving optimal therapeutic results. Thermal dose has been identified as one of the most important factors which, influences the efficacy of hyperthermia [Perez and Sapareto (1984)]. Although there are definite prescriptions for temperature (generally 43 ℃) and time (usually 60 min), variations in the temperature and time of delivery are frequent throughout the treatment sessions [Perez and Sapareto (1984), Jordan *et al.* (1999), Jordan *et al.* (2001), Overgaard *et al.* (2009)].

The effectiveness of hyperthermia treatment is related to the temperature achieved during the treatment. An ideal hyperthermia treatment should selectively destroy the tumor cells without damaging the surrounding healthy tissue. [Andrä *et al.* (1999), Lagendijk (2000), Moroz *et al.* (2002), Maenosono and Saita (2006), Lin and Liu (2009)]. Therefore, the ability to predict the temperature distribution inside as well as outside the target region as a function of the exposure time, possesses a high degree of importance.

In the past fifteen years, MFH has drawn greater attention due to the potential advantages for cancer hyperthermia therapy. In MFH, a nanofluid containing the MNPs is injected directly into the tumor. An alternating magnetic field is then applied to the target region, and then MNPs generate heat according to Néel relaxation and Brownian rotation losses as localized heat sources [Jordan *et al.* (1999), Jordan *et al.* (2001), Thiesen and Jordan (2008)]. The heat generated increases the temperature of the tumor. In general, the cancerous cells possess a higher chance to die when the temperature is above 43 ℃ whereas healthy cells will be safe at this temperature [Andrä *et al.* (1999), Moroz *et al.* (2002)].

Two techniques are currently used to deliver the MNPs to the tumor. The first is to deliver particles to the tumor vasculature [Matsuki and Yanada (1994)] through its supplying artery; however, this method is not effective for poorly perfused tumors. Furthermore, for a tumor with an irregular shape, inadequate MNPs distribution may cause under-dosage of heating in the tumor or overheating of the normal tissue. The second approach, is to directly inject MNPs into the extracellular space in the tumors. The MNPs diffuse inside the tissue after injection of nanofluid. If the tumor has an irregular shape, multi-site injection can be exploited to cover the entire target region [Salloum *et al.* (2008a)].

The nanofluid injection volume as well as infusion flow rate of nanofluid are important factors in dispersion and concentration of the MNPs, within the tissue. A successful MFH treatment is substantially dependent on the MNPs distribution in the tissue [Bagaria and Johnson (2005), Salloum *et al.* (2008a), Salloum *et al.* (2008b), Lin and Liu (2009), Bellizzi and Bucci (2010), Golneshan and Lahonian (2011a)].

2. Heat dissipation of MNPs

In MFH, after introducing the MNPs into the tumor (Figure 1), an alternating magnetic field is applied. This causes an increase in the tumor temperature and subsequent tumor regression. The temperature that can be achieved in the tissue strongly depends on the properties of the magnetic material used, the frequency and the strength of the applied magnetic field, duration of application of the magnetic field, and dispersion of the MNPs within the tissue.

2.1. Mechanisms of heat dissipation of MNPs

To turn MNPs into heaters, they are subjected to an oscillating electromagnetic field, where the field's direction changes cyclically. There are various theories which explain the reasons for the heating of the MNPs when subjected to an oscillating electromagnetic field [Brusentsova *et al.* (2005), Jo´zefczak and Skumiel (2007), Kim *et al.* (2008), Golneshan and Lahonian (2010), Golneshan and Lahonian (2011c)].

There exist at least four different mechanisms by which magnetic materials can generate heat in an alternating field [Nedelcu (2008)]:

1. Generation of eddy currents in magnetic particles with size >1μ,
2. Hysteresis losses in magnetic particles >1μ and multidomain MNPs,
3. Relaxation losses in 'superparamagnetic' single-domain MNPs,
4. Frictional losses in viscous suspensions.

Relaxation losses in single-domain MNPs fall into two modes: rotational (Brownian) mode and Néel mode. The principle of heat generation due to each individual mode is shown in Figure 2.

In the Néel mode, the magnetic moment originally locked along the crystal easy axis rotates away from that axis towards the external field. The Néel mechanism is analogous to the hysteresis loss in multi-domain MNPs whereby there is an 'internal friction' due to the

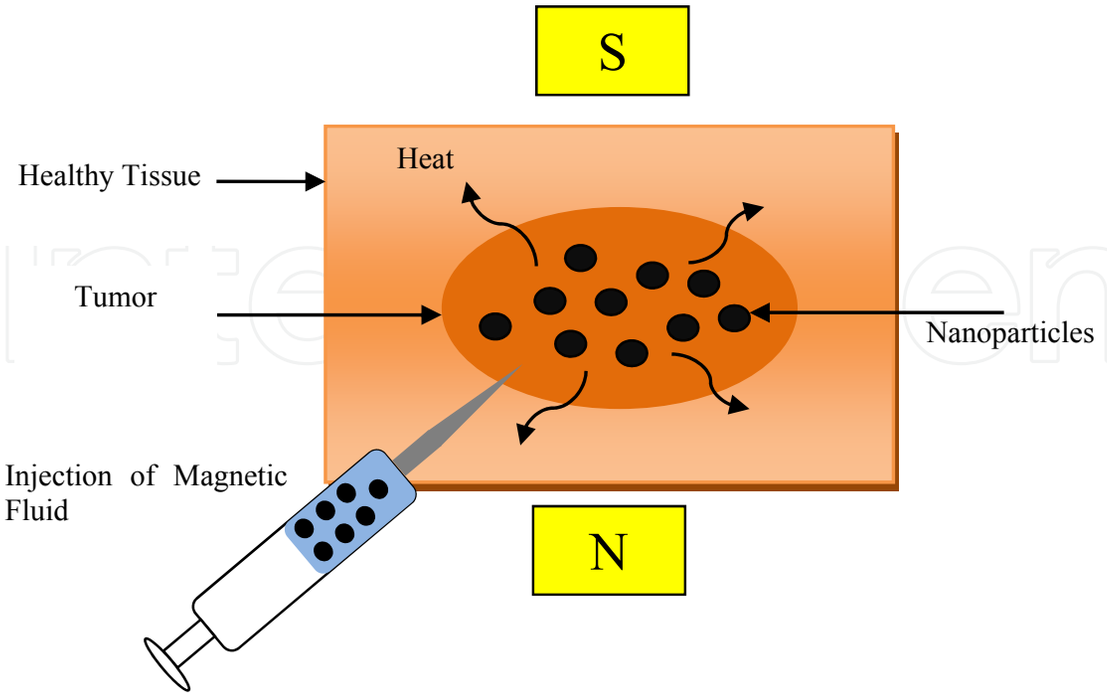

Figure 1. Schematic of magnetic fluid hyperthermia process.

movement of the magnetic moment in an external field that results in heat generation. In the Brownian mode, the whole particle oscillates towards the field with the moment locked along the crystal axis under the effect of a thermal force against a viscous drag in a suspending medium. This mechanism essentially represents the mechanical friction component in a given suspending medium [Nedelcu (2008)].

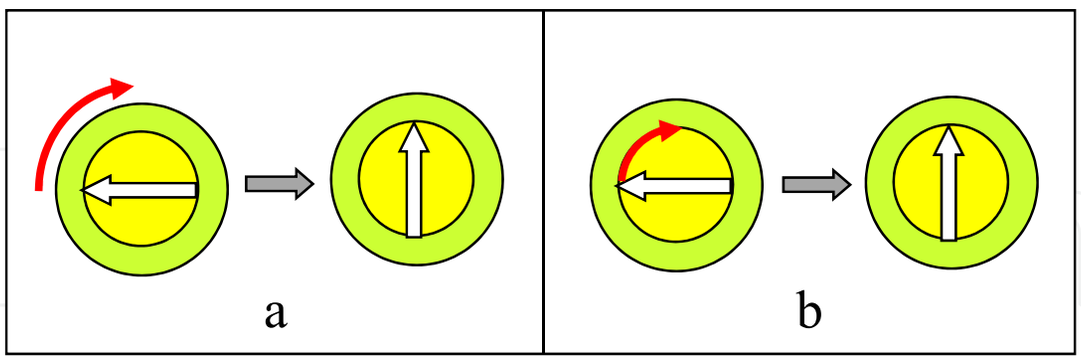

Figure 2. Relaxation mechanisms of MNPs in Magnetic Fluid. a) Brownian relaxation, entire particle rotates in fluid; b) Néel relaxation, direction of magnetization rotates in core. The structure of MNP: core (inner), shell (outer). The arrow inside the core represents the direction of magnetization.

Power dissipation of MNPs in an alternating magnetic field is expressed as [Rosensweig (2002), Nedelcu (2008)]:

$$P = \pi \mu_0 x_0 H_0^2 f \frac{2\pi f \tau}{1 + (2\pi f \tau)^2} \quad (1)$$

where μ_0 $(4\pi.10^{-7}\,T.m/A)$ is the permeability of free space, x_0 is the equilibrium susceptibility, H_0 and f are the amplitude and frequency of the alternating magnetic field and τ is the effective relaxation time, given by:

$$\tau^{-1} = \tau_N^{-1} + \tau_B^{-1} \tag{2}$$

where τ_N and τ_B are the Néel relaxation and the Brownian relaxation time, respectively. τ_N and τ_B are written as:

$$\tau_N = \frac{\sqrt{\pi}}{2}\tau_0 \frac{exp(\Gamma)}{\sqrt{\Gamma}} \tag{3}$$

$$\tau_B = \frac{3\eta V_H}{kT} \tag{4}$$

where the shorter time constant tends to dominate in determining the effective relaxation time for any given size of particle. τ_0 is the average relaxation time in response to a thermal fluctuation, η is the viscosity of medium, V_H is the hydrodynamic volume of MNPs, k is the Boltzmann constant, 1.38×10^{-23} J/K, and T is the temperature. Here, $\Gamma = KV_M/\,kT$ where K is the magnetocrystalline anisotropy constant and V_M is the volume of MNPs. The MNPs volume V_M and the hydrodynamic volume including the ligand layer V_H are written as:

$$V_M = \frac{\pi D^3}{6} \tag{5}$$

$$V_H = \frac{\pi(D + 2\delta)^3}{6} \tag{6}$$

where D is the diameter of MNP and δ is the ligand layer thickness.

The equilibrium susceptibility x_0 is assumed to be the chord susceptibility corresponding to the Langevin equation ($L(\xi) = M/M_s = \coth\xi - 1/\xi$), and expressed as:

$$x_0 = x_i \frac{3}{\xi}\left(\coth\xi - \frac{1}{\xi}\right) \tag{7}$$

where $\xi = \mu_0 M_d H V_M/kT$, $H = H_0 cos(\omega t)$, $M_s = \phi M_d$, and ϕ is the volume fraction of MNPs. Here, M_d and M_s are the domain and saturation magnetization, respectively. The initial susceptibility is given by:

$$x_i = \frac{\mu_0 \phi M_d^2 V_M}{3kT} \tag{8}$$

Generally, the practical range of frequency and amplitudes are often described as $50 - 1200\ kHz$ and $0 - 15\ kA/m$ and the typical magnetite dosage is $\sim 10\ mg$ magnetite MNPs per gram of tumor as reported in clinical studies [Jordan *et al.* (1997), Jordan *et al.* (2001), Pankhurst *et al.* (2003), Lahonian and Golneshan (2011)].

2.2. Heating rate of aqueous dispersions of MNPs

Based on the theory mentioned in previous section, Lahonian and Golneshan (2011) calculated the power dissipations for aqueous dispersion of mono-dispersed equiatomic face centred cubic iron-platinum (FCC FePt) MNPs varying the diameter of MNP in adiabatic condition. For comparison, also the power dissipations for magnetite (Fe_3O_4), and maghemite (γ-Fe_2O_3) have been estimated. In Table 1, physical properties of each magnetic material are shown [Maenosono and Saita (2006)].

In practice, the magnetic anisotropy may considerably vary due to the shape contributions of MNPs. For simplicity, however, the shape effect is not taken into account in the above mentioned model.

It has been pointed out that hysteresis losses are important especially for magnetic single domain particles with high magneto-crystalline anisotropy [Hergt *et al.* (1998)]. However, the hysteresis losses are not considered, because MNPs are assumed as super-paramagnetic in their study.

Figure 3 shows comparative power dissipation for aqueous mono-dispersions of the various MNPs listed in Table 1, assuming $\tau_0 = 10^{-9}\ s$ and $\phi = 2 \times 10^{-5}$. Induction and frequency of applied magnetic field were fixed at $B_0 = \mu_0 H_0 = 50\ mT$ and $300\ kHz$. The carrier liquid is pure water in all cases. Surface ligand layer thickness is assumed to be $\delta = 1\ nm$. On these conditions, FCC FePt MNPs yield the largest power dissipation. Most operative sizes of each MNPs, D_{max}, which give a maximum heating rate, are $10.5\ nm$ for FCC FePt MNPs, $19\ nm$ for magnetite and $23\ nm$ for maghemite. The maghemite MNPs also have large power dissipation as well as magnetite MNPs. The typical size ranges of standard magnetic nanofluid are $D = 8 - 10\ nm$, and generally the stability of magnetic colloid becomes impaired when $D > 20\ nm$ due to the spontaneous magnetization [Golneshan and Lahonian (2010), Lahonian and Golneshan (2011), Golneshan and Lahonian (2011b).

Figure 4 shows the dependence of power dissipation on induction of applied magnetic field, for fixed $f = 300\ kHz$. Note that B_0 is varied as 30, 50, and $80\ mT$. Increasing B_0 earns a raise for power dissipation [Lahonian and Golneshan (2011)].

Figures 5, 6 and 7 show the dependence of power dissipation on the frequency (f), the surface ligand layer thickness (δ), and the volume fraction (ϕ) respectively. Increasing f earns a raise and a gradual decrease, respectively, in the power dissipation and D_{max}. The power dissipation decreases and increases with increasing δ and ϕ, respectivly. Also, the gradual decrease in D_{max} with decreasing δ is observed [Lahonian and Golneshan (2011)].

Material	M_d kA/m	K kJ/m^3	c_p $J/(kg.K)$	ρ kg/m^3
FCC FePt	1140	206	327	15200
Magnetite	446	9	670	5180
Maghemite	414	4.7	746	4600

Table 1. Physical properties of various MNPs [Maenosono and Saita (2006)]

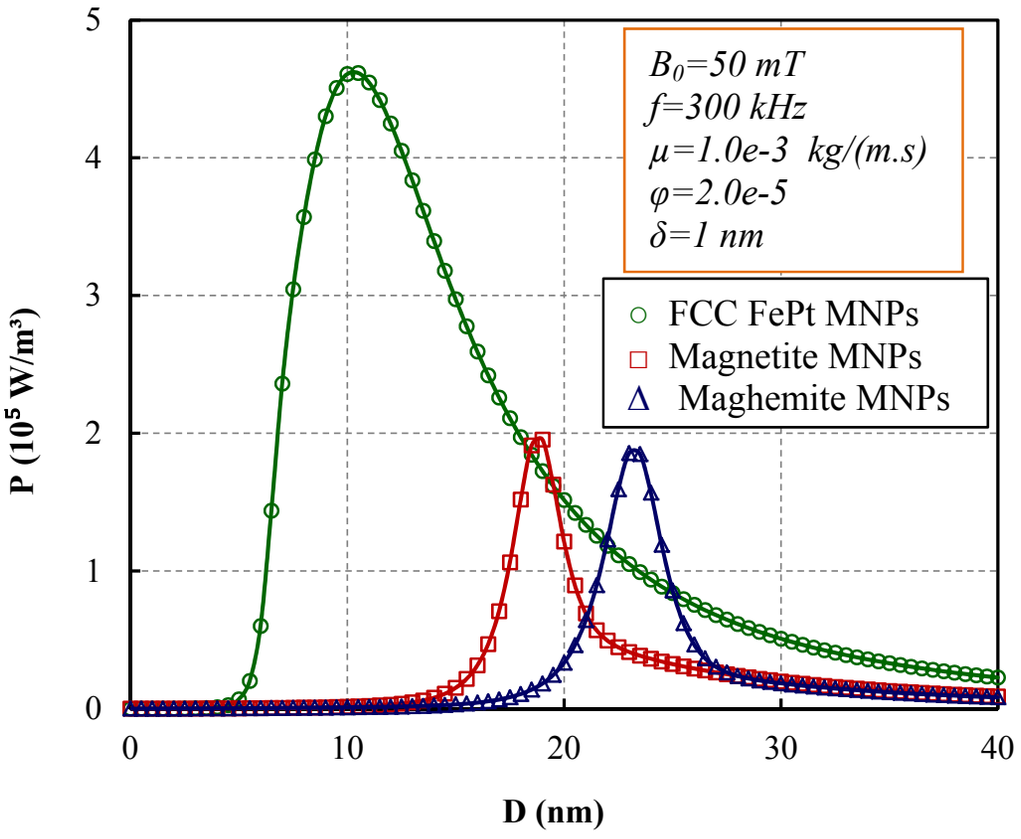

Figure 3. Power dissipations as a function of particle diameter for various MNPs [Lahonian and Golneshan (2011)].

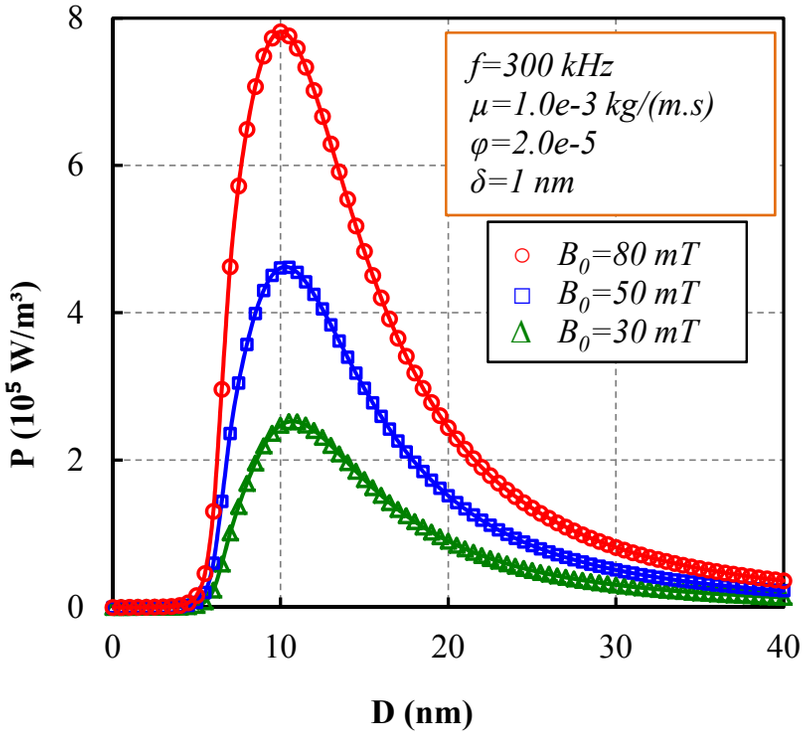

Figure 4. Dependence of power dissipation on B_0 [Lahonian and Golneshan (2011)].

Figures 4 to 7 show that dispersion and concentration of MNPs inside the tissue are important factors in heat dissipation of MNPs and temperature distribution inside the tumor and its surrounding healthy tissue. Also, the effect of concentration of MNPs is comparable with the effects of induction and frequency of the magnetic field on the maximum power dissipation. Therefore, study of the MNPs diffusion and concentration, possesses a high degree of importance.

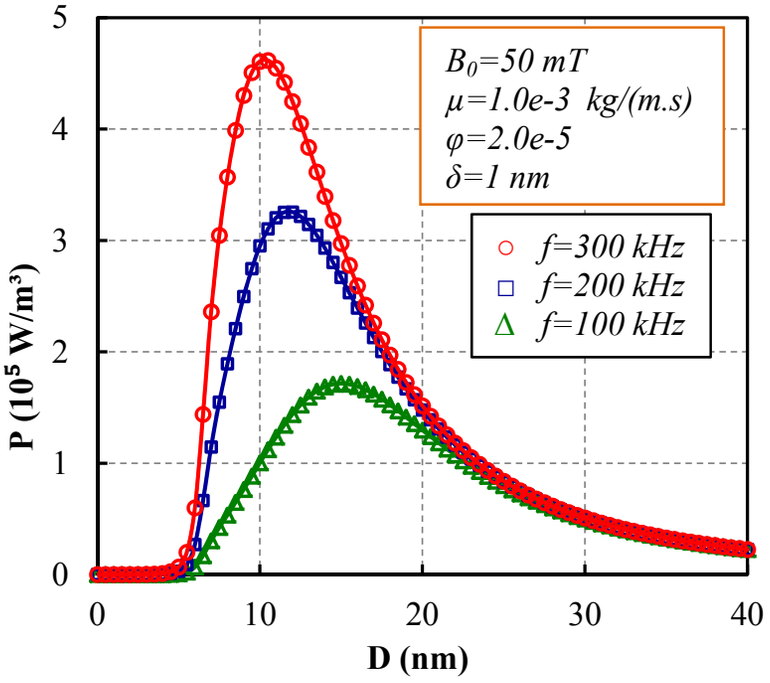

Figure 5. Dependence of power dissipation on f [Lahonian and Golneshan (2011)].

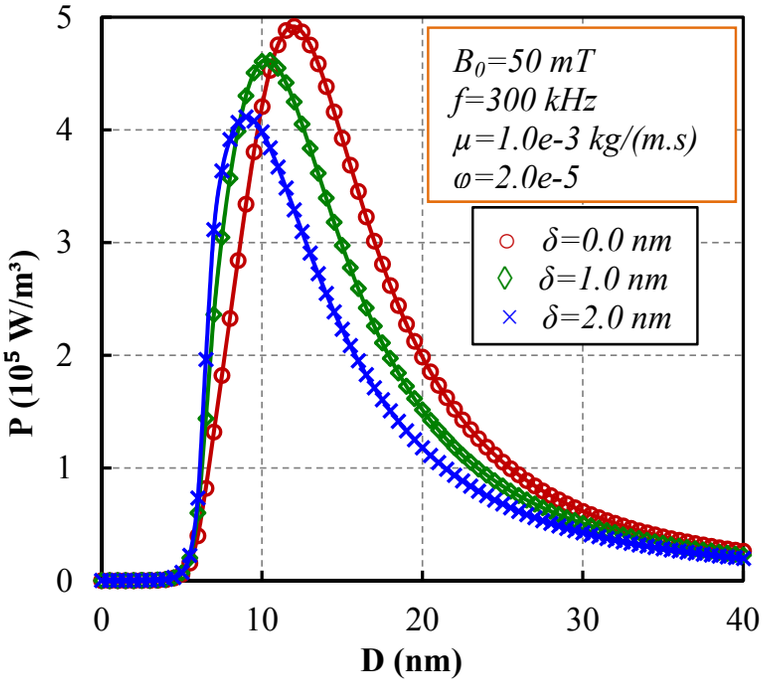

Figure 6. Dependence of power dissipation on δ [Lahonian and Golneshan (2011)].

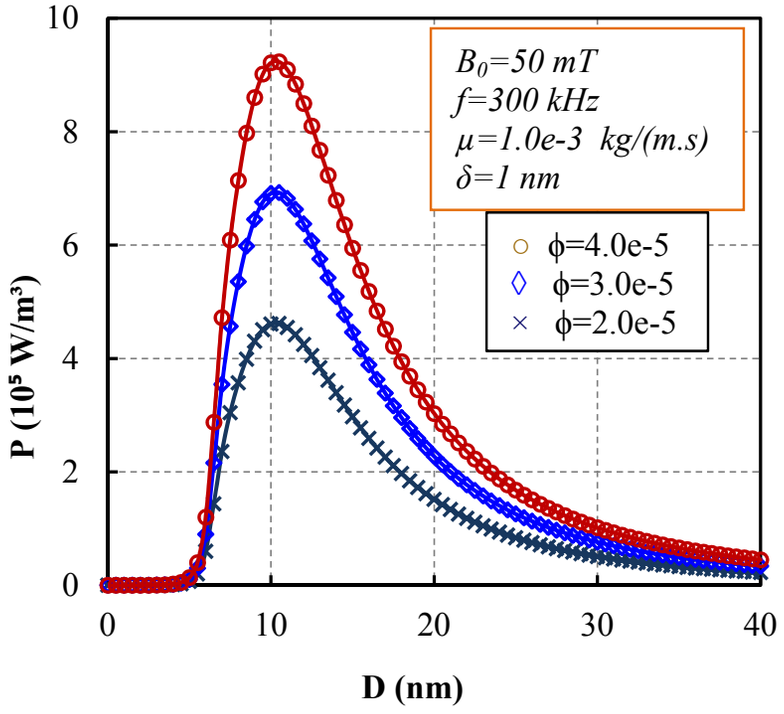

Figure 7. Dependence of power dissipation on ϕ [Lahonian and Golneshan (2011)].

3. Diffusion of MNPs within the biological tissue

The relationship among the MNPs distribution, the blood perfusion, the infusion flow rate, the injection volume of nanofluid, and the tissue structure are not well understood. It is difficult to devise a treatment protocol that enables the optimum distribution of temperature elevation in the tumor. Hence, it is important to quantify the MNPs distribution and heating pattern following the injection regarding the above mentioned factors [Salloum *et al.* (2008b)].

Diffusion in isotropic tissues, can be modeled as [Nicholson (2001)]:

$$\frac{\partial C}{\partial t} = \mathrm{D}^{*}\nabla^2 C + S/\varepsilon \tag{9}$$

where C, D^*, S, ε and t are the volume average concentration of the species, effective diffusivity, mass source density, porosity of the tissue and time, respectively. The effective diffusivity, however, is related to the tortuosity of the tissue, λ, and the diffusivity in the absence of the porous medium, D through the following relation:

$$D^* = D/\lambda^2 \tag{10}$$

Therefore an increase in the tortuosity and a decrease in the porosity have significant effects on reducing the effective mass diffusivity.

Experimental study of Salloum *et al.* (2008a) in a tissue-equivalent agarose gel, showed that the particle concentration was not uniform after the injection and were confined in the

vicinity of the injection site. Also the particle deposition was greatly affected by the injection rate and amount. Furthermore, the shape of the distribution tended to be more irregular with higher infusion flow rate.

Due to difficulties in experimental studies, to understand the actual spatial distribution of the MNPs after being injected into the tumor, some numerical simulations have been down.

Diffusion of MNPs inside the tissue was simulated by Golneshan and Lahonian (2011a). A square region with side of 2 cm was chosen as the domain of the analysis (Figure 8). Water-based ferrofluid with a concentration of 3.3% by volume and a particle size of 10 nm magnetite MNPs was used in their work. Based on the density of magnetite (5240 kg/m^3) and the given ferrofluid concentration, each 0.1 cc of ferrofluid contains 17.3mg of solid iron oxide [Golneshan and Lahonian (2010)]. The ferrofluid infusion flow rates were chosen equal to $\dot{V} = 10, 20$ and 30 $\mu l/min$ and ferrofluid injection volumes were chosen equal to $V = 0.1, 0.2$ and 0.3 cc. Porosity and effective diffusivity were chosen to be equal to $\varepsilon = 0.1$ and $D^* = 2.5 \times 10^{-10}\ m^2/s$ respectively [Nicholson (2001), Golneshan and Lahonian (2010)].

Figure 9 shows the concentration of ferrofluid in the tissue for $V = 0.2\ cc$ and $\dot{V} = 20\ \mu l/min$, for different time intervals after the end of ferrofluid injection. Results show that the concentration of ferrofluid is maximum at the injection site, and decreases rapidly with increasing distance from it. Also, concentration of ferrofluid decreases at the injection area with time and increases in the surrounding of injection site [Golneshan and Lahonian (2011a)].

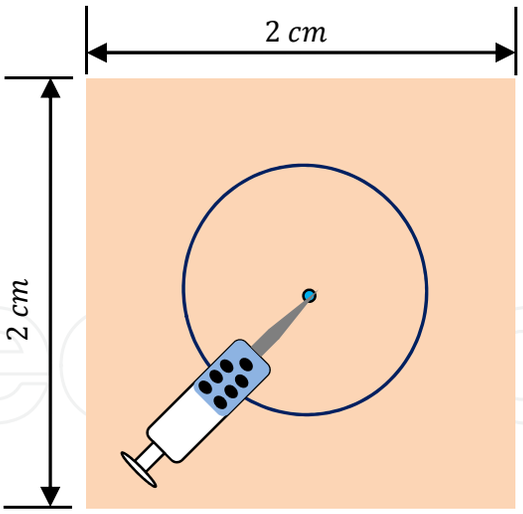

Figure 8. Simulation domain of tissue and injection site.

Figure 10 shows volume fraction of MNPs in the tissue for different ferrofluid injection volumes, $\dot{V} = 20\ \mu l/min$, at 20 minutes after the end of ferrofluid injection [Golneshan and Lahonian (2011a)].

Figure 11 shows the concentration of ferrofluid in the tissue for $V = 0.2\ cc$, and different infusion flow rates, just 20 minutes after the end of ferrofluid injection. Results show that

the increasing infusion flow rate, increases concentration of ferrofluid in the vicinity of the injection site while decreasing the concentration in the layers far from the injection site [Golneshan and Lahonian (2011a)].

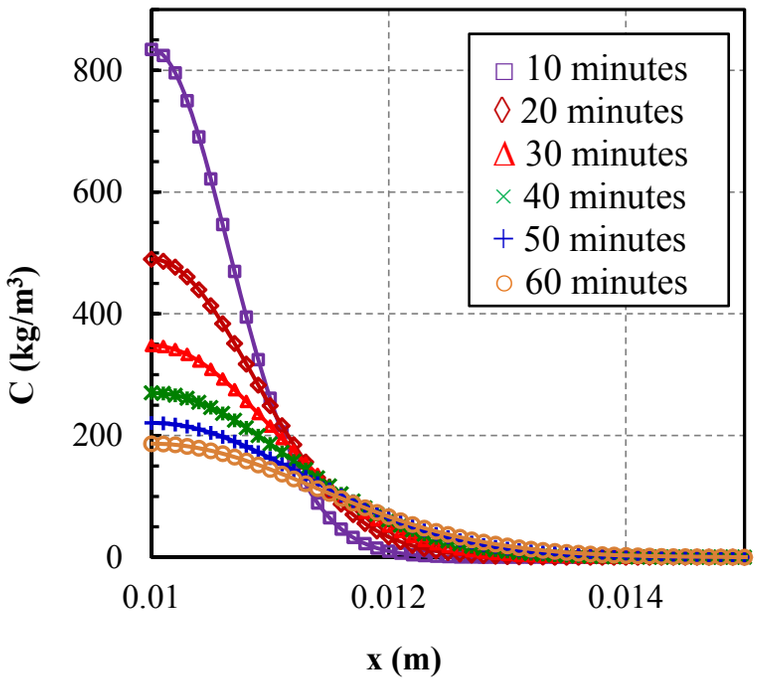

Figure 9. Concentration of ferrofluid in the tissue, for different time intervals after the end of ferrofluid injection ($V = 0.2\ cc$ and $\dot{V} = 20\ \mu l/min$) [Golneshan and Lahonian (2011a)].

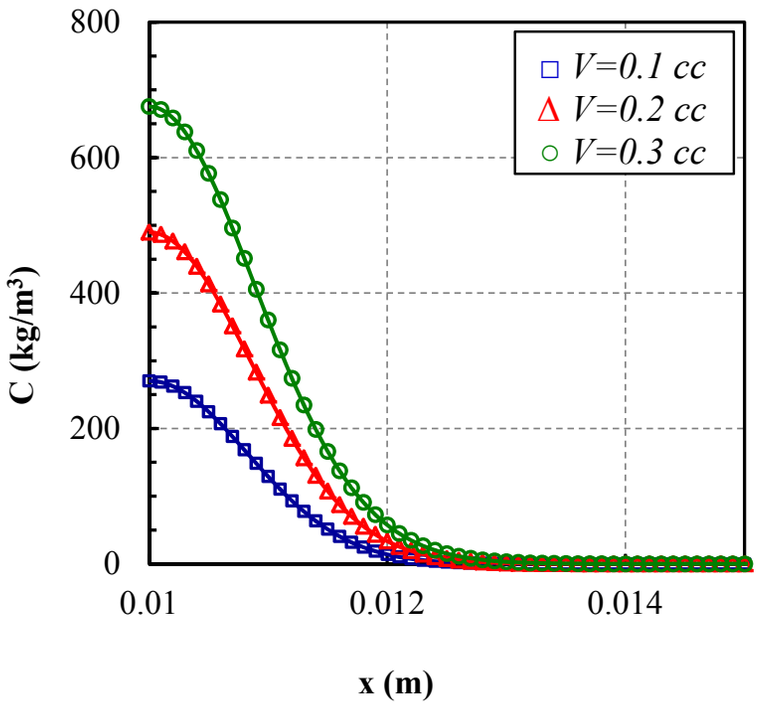

Figure 10. Ferrofluid concentration for $\dot{V} = 20\ \mu l/min$, and different ferrofluid injection volumes, just 20 minutes after the end of ferrofluid injection [Golneshan and Lahonian (2011a)].

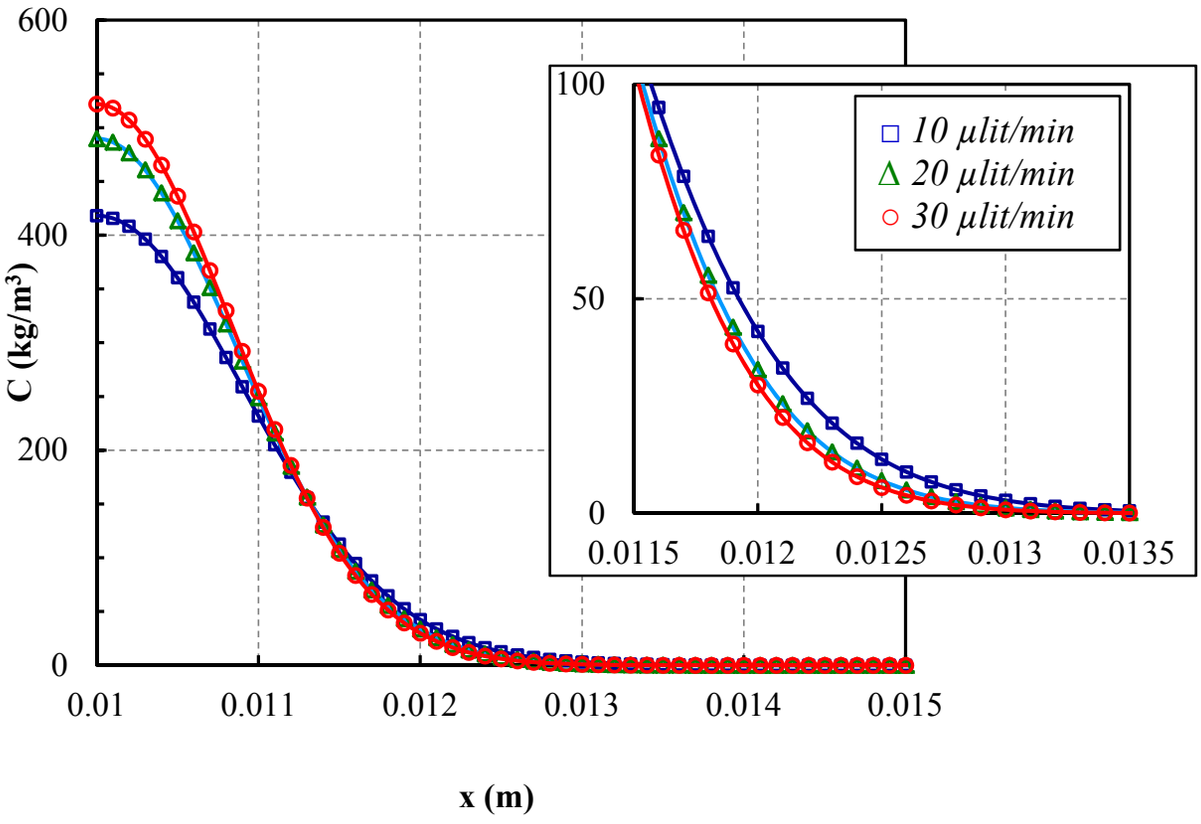

Figure 11. Concentration of ferrofluid in the tissue for $V = 0.2\ cc$, and different infusion flow rates, just 20 minutes after the end of ferrofluid injection [Golneshan and Lahonian (2011a)].

Figure 12 shows the concentration of ferrofluid in the tissue for $V = 0.2\ cc$, and different infusion flow rates, just 20 minutes after the end of ferrofluid injection. Results show that the increasing infusion flow rate, increases concentration of ferrofluid in the vicinity of the injection site but decreases the concentration in the layers far from the injection site [Golneshan and Lahonian (2010), Golneshan and Lahonian (2011a)].

4. Diffusion of MNPs in a biological tissue for mono and multi-site injection for irregular tumors

Golneshan and Lahonian (2011a) studied diffusion of MNPs in a biological tissue for irregular tumors. A $2 \times 2\ cm$ tissue with an irregular tumor inside, was chosen as the domain of the analysis (Figures 13a).

They considered multi-site injection as shown in Figure 13d and divided the irregular tumor almost into four equal sections. In each injection site, one fourth the amount of $0.2\ cc$ ferrofluid was injected. Figure 14 shows the concentration of ferrofluid for infusion flow rate of $\dot{V} = 20\ \mu l/min$, at the end of ferrofluid injection [Golneshan and Lahonian (2011a)].

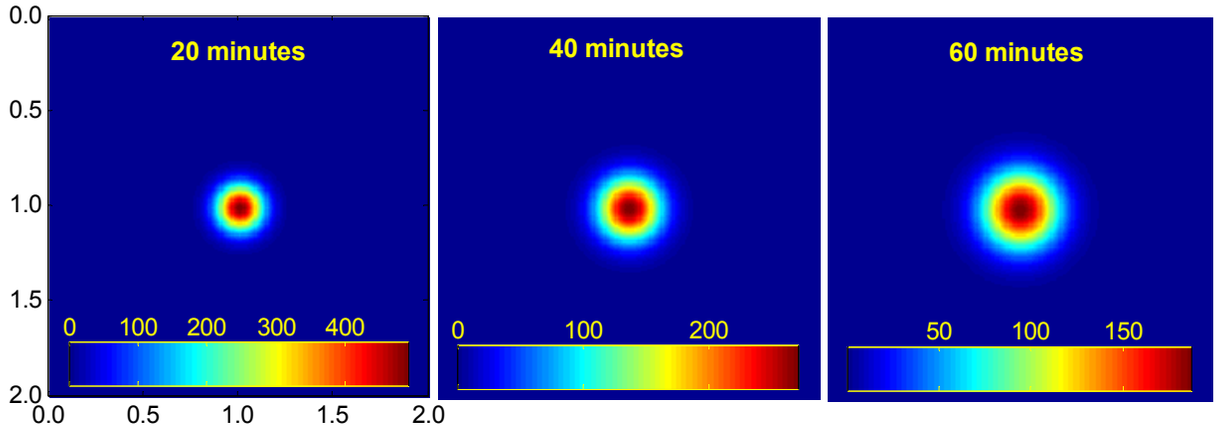

Figure 12. Concentration of ferrofluid in kg/m^3 in the tissue for $V = 0.2\ cc$, $\dot{V} = 20\ \mu l/min$, at 20, 40 and 60 minutes after the end of ferrofluid injection [Golneshan and Lahonian (2011a)].

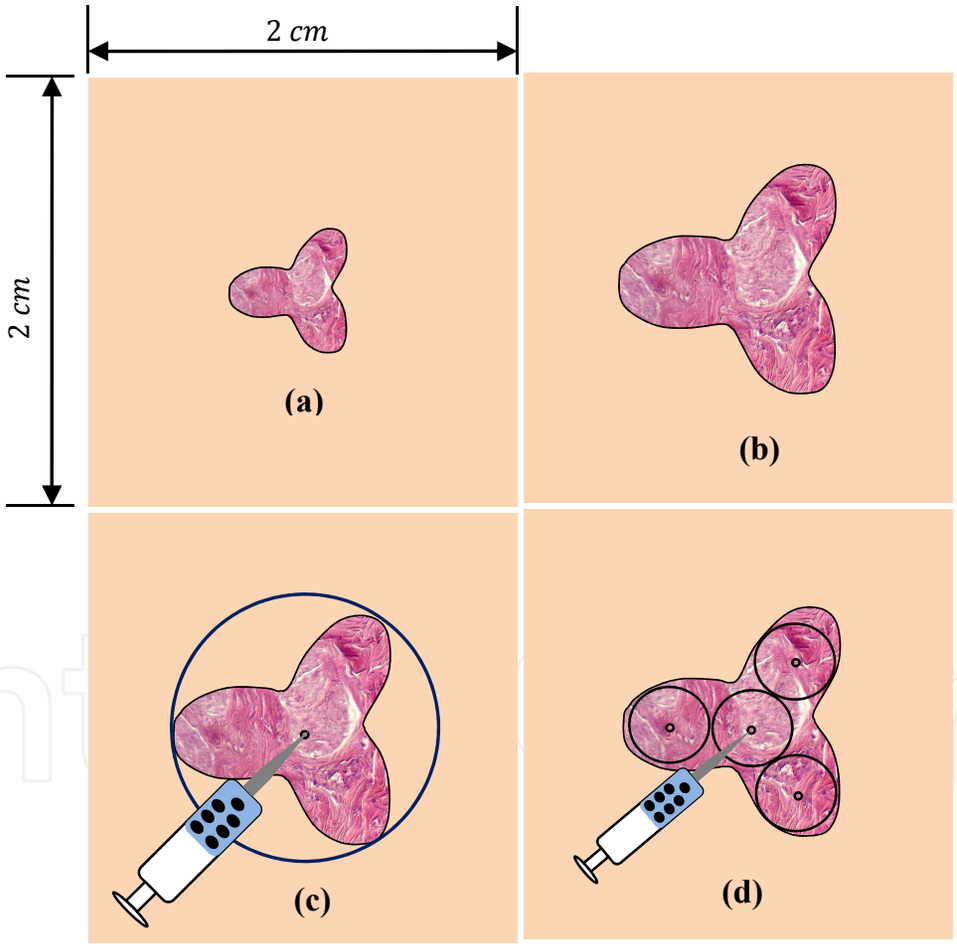

Figure 13. a: The tissue and an irregular tumor, b: Zoomed irregular tumor c: Mono-site injection, d: Multi-site injection [Golneshan and Lahonian (2011a)].

Figure 15 shows the concentration of ferrofluid in kg/m^3 in the tissue for mono and multi-site injection of $V = 0.2\ cc$ ferrofluid injection volume and infusion flow rate of $\dot{V} = 20\ \mu l/min$, at 10, 20, and 30 minutes after the end of ferrofluid injection. Ten minutes after

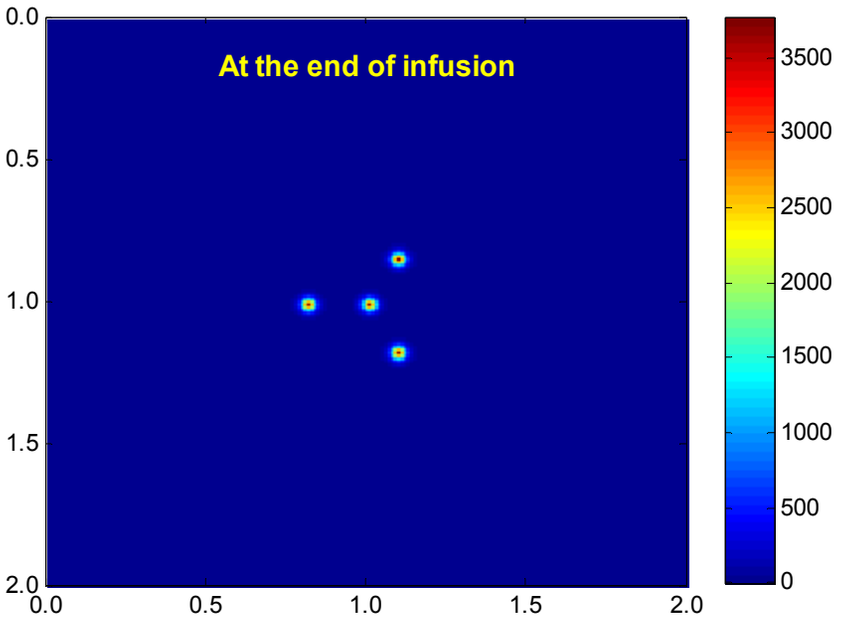

Figure 14. Concentration of ferrofluid in kg/m^3 for multi-site injection, at the end of injection process [Golneshan and Lahonian (2011a)].

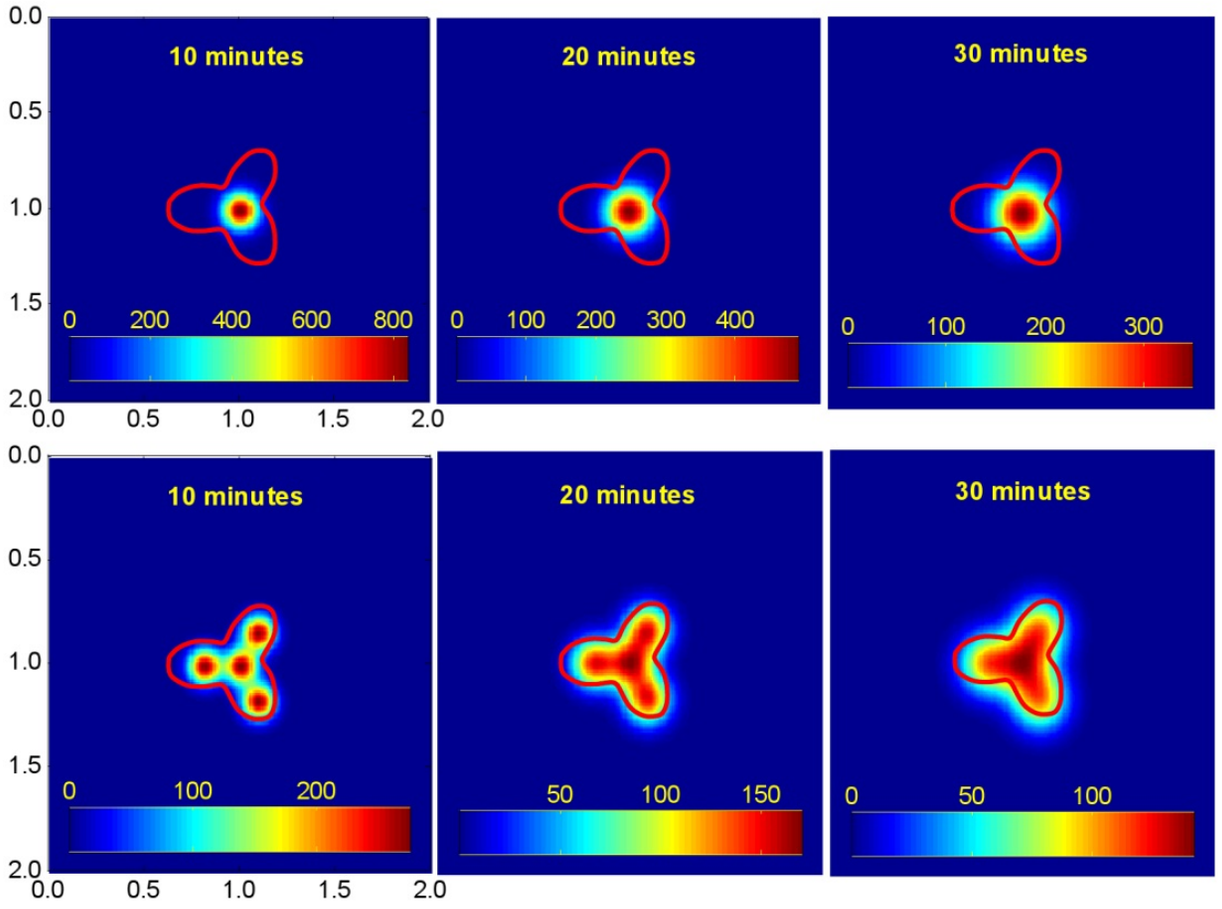

Figure 15. Concentration of ferrofluid in kg/m^3 in the tissue for $V = 0.2\ cc$, $\dot{V} = 20\ \mu l/min$, at 10, 20 and 30 minutes after the end of ferrofluid injection. Up row: Mono-site injection, Down row: Multi-site injection [Golneshan and Lahonian (2011a)].

the injection, the maximum concentration of ferrofluid happens at the injection sites, decreasing rapidly with increasing the distance from the injection sites. At this stage, nearly clear boundaries are seen between diffused ferrofluid for each injection regions. As ferrofluid diffuses more and more, these boundaries are disappeared. Thirty minutes after the injection, the ferrofluid is spread all over the tomour [Golneshan and Lahonian (2011a)].

Comparison between mono-site and multi-site injections in Figures 15 show that diffusion of ferrofluid in the tissue for a multi-site injection is much more uniform and covers all points inside the tumor 30 minutes after the end of injection process. Furthermore, no substantial concentration gradient is seen between the center and the boundary of the tumor at this time for the multi-site injection case [Golneshan and Lahonian (2011a)].

5. Conclusion

Results showed and clarified that increasing the magnetic nanofluid injection volume, increases the concentration of MNPs inside the tissue. Also, increasing magnetic nanofluid infusion flow rate increased the concentration of MNPs in the center of the tumor only. For irregular tumors, the effect of multi-site injection was investigated. Results showed that multi-site injection of specific quantity of magnetic nanofluid provided a better distribution of MNPs inside the tumor, in contrast to mono-site injection.

Author details

Mansour Lahonian
Mechanical Engineering Department, Engineering School, Kurdistan University, Sanandaj, Iran

6. References

Andrä W, C G D'Ambly, R Hergt, I Hilger, W A Kaiser (1999). Temperature distribution as function of time around a small spherical heat source of local magnetic hyperthermia. *J Magn Magn Mater* 194:197–203.

Bagaria H G, and D T Johnson (2005). Transient solution to the BHE and optimization for magnetic fluid hyperthermia treatment *Int J Hyperther* 21(1): 57–75.

Bellizzi G, O M Bucci (2010). On the optimal choice of the exposure conditions and the nanoparticle features in magnetic nanoparticle hyperthermia *Int J Hyperther* 26:389-403.

Brusentsova T N, N A Brusentsov, V D Kuznetsov, V N Nikiforov (2005). Synthesis and investigation of magnetic properties of Gd-substituted Mn–Zn ferrite nanoparticles as a potential low-TC agent for magnetic fluid hyperthermia *J Magn Magn Mater* 293: 298-302.

Golneshan A A, M Lahonian (2010). Diffusion of magnetic nanoparticles within spherical tissue as a porous media during magnetic fluid hyperthermia using lattice Boltzmann method *International Congress on Nanoscience and Nanotechnology* 9-11 November, shiraz iran.

Golneshan A A, M Lahonian (2011a). Diffusion of magnetic nanoparticles in a multi-site injection process within a biological tissue during magnetic fluid hyperthermia using lattice Boltzmann method *Mech Res Commun* 38: 425– 430.

Golneshan A A, M Lahonian (2011b). Effect of heated region on temperature distribution within tissue during magnetic fluid hyperthermia using lattice Boltzmann method *Journal of Mechanics in Medicine and Biology* 11(2):457–469.

Golneshan A A, M Lahonian (2011c). The effect of magnetic nanoparticle dispersion on temperature distribution in a spherical tissue in magnetic fluid hyperthermia using the lattice Boltzmann method *Int J Hypertherm* 27(3):266–274.

Hergt R, W Andrä, C G d'Ambly, I Hilger, W A Kaiser, U Richter, H-G Schmidt (1998). Physical limits of hyperthermia using magnetite fine particles *IEEE T Magn* 5: 3745–3754.

Jo´zefczak A, A Skumiel (2007). Study of heating effect and acoustic properties of dextran stabilized magnetic fluid *J Magn Magn Mater* 311: 193–196.

Jordan A, R Scholz, K Maier-Hauff, M Johannsen, P Wust, J Nadobny, H Schirra, H Schmidt, S Deger, S Loening, W Lanksch, R Felix (2001). Presentation of a new magnetic field therapy system for the treatment of human solid tumors with magnetic fluid hyperthermia *J Mag Mag Mater* 225: 118-126.

Jordan A, R Scholz, P Wust, H Fähling, J Krause, W Wlodarczyk,B Sander, T Vogl, R Felix (1997). Effect of magnetic fluid hyperthermia on C3H mammary carcinoma in vivo *Int J Hypertherm* 13:587–605.

Jordan A, R Scholz, P Wust, H Schirra, T Schiestel, H Schmidt, R Felix (1999). Endocytosis of dextran and silan-coated magnetite nanoparticles and the effect of intracellular hyperthermia on human mammary carcinoma cells in vitro *J Magn Magn Mater* 194: 185–196.

Kim D H, D E Nikles, D T Johnson, C S Brazel (2008). Heat generation of aqueously dispersed CoFe2O4 nanoparticles as heating agents for magnetically activated drug delivery and hyperthermia *J Magn Magn Mater* 320: 2390– 2396.

Lagendijk J J W (2000). Hyperthermia treatment planning *Phys Med Biol* 45:R61–R76.

Lahonian M. A A Golneshan (2011). Numerical study of temperature distribution in a spherical tissue in magnetic fluid hyperthermia using lattice Boltzmann method *IEEE Trans Nanobio* 10(4): 262-268.

Lin Ch T, Liu K Ch (2009). Estimation for the heating effect of magnetic nanoparticles in perfused tissues *Int Commun Heat Mass* 36: 241–244.

Maenosono S, S Saita (2006). Theoretical assessment of FePt nanoparticles as heating elements for magnetic hyperthermia *IEEE T Magn* 42: 1638–1642.

Matsuki H, T Yanada (1994). Temperature sensitive amorphous magnetic flakes for intra-tissue hyperthermia *Mat Sci Eng A-Struct* 181/A182: 1366–1368.

Moroz P, S K Jones, B N Gray (2002). Magnetically mediated hyperthermia: Current status and future directions *Int J Hyperther* 18: 267–284.

Nedelcu G (2008). Magnetic nanoparticles impact on tumoural cells in the treatment by magnetic fluid hyperthermia *Digest J Nanomat Biost* 3(3): 103–107.

Nicholson C (2001). Diffusion and related transport mechanism in brain tissue *Rep Prog Phys* 64: 815–884.

Overgaard J, D Gonzalez, M C C H Hulshof, G Arcangeli, O Dahl, O Mella, S M Bentzen (2009). Hyperthermia as an adjuvant to radiation therapy of recurrent or metastatic malignant melanoma. A multicentre randomized trial by the European Society for Hyperthermic Oncology *Int J Hyperther* 25: 323-334.

Pankhurst QA, J Connolly, S K Jones, J Dobson (2003). Application of magnetic nanoparticles in biomedicine *J Phys D Appl Phys* 36:R167–R187.

Perez C A, S A Sapareto (1984). Thermal dose expression in clinical hyperthermia and correlation with tumor response/control1 *Cancer Res* 44: 4818-4825.

Rosensweig R E (2002). Heating magnetic fluid with alternating magnetic field *J Magn Magn Mater* 252: 370-374.

Salloum M, R H Ma, D Weeks, L Zhu (2008a). Controlling nanoparticle delivery in magnetic nanoparticle hyperthermia for cancer treatment: Experimental study in agarose gel *Int J Hyperther* 24: 337–345.

Salloum M, R H Ma, L Zhu (2008b). An in-vivo experimental study of temperature elevations in animal tissue during magnetic nanoparticle hyperthermia *Int J Hyperther* 24: 589-601.

Thiesen B, A Jordan (2008). Clinical applications of magnetic nanoparticles for hyperthermia *Int J Hyperther* 24: 467-474.